PHYSICAL REVIEW B **75**, 092103 (2007)

Silver molybdate nanoparticles, nanowires, and nanorods embedded in glass nanocomposites

S. Bhattacharya and A. Ghosh*
Department of Solid State Physics and DST Unit on Nano Science, Indian Association for the Cultivation of Science, Jadavpur, Kolkata 700032, India

(Received 24 January 2007; published 30 March 2007)

Formation of $Ag_6Mo_{10}O_{33}$ nanowires, Ag_2MoO_4 nanoparticles, and $Ag_2Mo_2O_7$ nanorods embedded in silver molybdate glassy matrix has been confirmed from x-ray diffraction, field-emission scanning electron microscopy, and high-resolution transmission electron microscopy studies. Heat-treated samples with higher Ag_2O content are good templates for the formation of the above-mentioned nanophase structures of definite geometric shape and size. The $Ag_2Mo_2O_7$ nanorodlike structures do not change in length effectively but their changes in width are noteworthy with the increase of Ag_2O content. Distribution of nanophases of different shapes and sizes was confirmed quantitatively from the crystalline lattice strain in the interface between the nanocrystals and the glass matrix. The initial rapid growth of the nanoparticles is also explained quantitatively with the help of a hit-and-stick model.

DOI: 10.1103/PhysRevB.75.092103 PACS number(s): 81.07.−b, 81.07.Bc

Nanostructured materials have been the subject of intense research recently because of their unusual physical properties and potential applications.[1,2] The synthesis of nanodots, nanowires, nanobelts, etc., of different materials has posed challenging tasks to materials scientists. Different physical and chemical methods have been used to grow nanomaterials in different forms.[3] Recently, the synthesis of low-dimensional metal molybdates such as MoO_3 nanorods[4] has attracted a lot of interest due to their strong application potential in various fields such as photoluminescence,[5] microwave applications,[6] optical fiber,[7] humidity sensor,[8] etc. Binary silver molybdate glass structure formed with unconventional glass former has a substantial amount of void space within it. Nanometer and/or micrometer-sized particles can be accommodated in these matrices. We have carried out the melt-quenching technique on selected silver molybdate glass matrix to grow the dispersed phase of $Ag_6Mo_{10}O_{33}$ nanowires, Ag_2MoO_4 nanoparticles, and $Ag_2Mo_2O_7$ nanorods of definite geometrical shapes in the host glass matrix.

Silver molybdate glasses are particularly interesting because of the growing evidence of anomalous structure as well as different intensive properties when compared with traditional silver phosphate, borate, and tellurite glasses,.[9–11] The molybdenum species exist in the glasses as tetrahedral orthomolybdate anion MoO_4^{-2}.[12–14] The existence of octahedral molybdenum environment has also been suggested.[15] Recent x-ray photoelectron spectroscopy (XPS) study[16] shows that the binding energy of molybdate glasses typically increases with an increase in the oxidation state of Mo ions.

In the present paper, we have reported the formation of Ag_2MoO_4 nanoparticles and $Ag_2Mo_2O_7$ nanorods dispersed in the silver molybdate glass nanocomposites. We have obtained single-crystalline $Ag_6Mo_{10}O_{33}$ nanowires, polycrystalline Ag_2MoO_4 nanoparticles, and $Ag_2Mo_2O_7$ nanorods embedded in the heat-treated samples. The hit-and-stick model is employed to explain quantitatively the initial rapid growth of the nanophase structures.

Glass samples of compositions $xAg_2O\text{-}(1-x)MoO_3$, where $x=0.2$, 0.3, and 0.4, were prepared from the reagent grade chemicals $AgNO_3$ and MoO_3. The mixtures of these chemicals in appropriate proportions were held at 400 °C for 2 h for denitrogination of $AgNO_3$ and melted in the temperature range from 650 to 700 °C depending on composition. The melts were equilibrated for 2 h and were finally quenched between two aluminum plates. Transparent glass samples with thickness of ~1 mm were obtained for $x=0.2-0.4$. The differential thermal analysis (DTA) was carried out to determine the glass transition temperature. The estimated glass transition temperatures (T_g) for the samples $x=0.2$, 0.3, and 0.4 are 290, 250, and 200 °C, respectively. The glass samples were then given a heat treatment at 50 °C over the glass transition temperature for 2 h. Formation of different nanophases such as nanoparticles, nanowires, and nanorods precipitated within the glasses was confirmed from x-ray-diffraction (SEIFERT XRD 3000P), field-emission scanning electron microscopic (JEOL JSM-6700F), and transmission electron microscopic (JEOL JEM 2010) studies and Fourier transform infrared (FT-IR) spectra (Nicolet MAGNA-IR 750).

X-ray-diffraction patterns of three sample compositions along with their heat-treated counterparts are shown in Fig. 1. The diffractograms of the compositions $x=0.2$ and 0.3 (Fig. 1, curves a and b) show broad diffuse scattering at low angle characteristic of long-range structural disorder, while the composition $x=0.4$ (Fig. 1, curve c) exhibits (220) and (440) peaks due to Ag_2MoO_4 and (020) and (200) peaks due to $Ag_2Mo_2O_7$ nanophase.[17] In the heat-treated samples, different silver molybdate nanophases grow depending on the compositions. The heat-treated sample $x=0.2$ [Fig. 1, curve d] exhibits (511) and (440) crystalline peaks corresponding to Ag_2MoO_4 cubic system of $Fd\bar{3}m$ space-group structure,[17,18] (020), $(\bar{1}12)$, (200), (012), (021), $(\bar{1}03)$, (121), and $(\bar{1}\bar{3}2)$ peaks due to $Ag_2Mo_2O_7$ and (011), $(\bar{1}\bar{1}2)$, (112), and $(\bar{1}\bar{1}5)$ due to $Ag_6Mo_{10}O_{33}$ crystal with $P1$ and $P\bar{1}$ space groups of triclinic symmetry, respectively.[19,20] (220), (511), and (440) peaks due to Ag_2MoO_4 cubic system,[17,18] (020), (200), and (121) peaks due to $Ag_2Mo_2O_7$, and two other peaks $(1\bar{2}2)$ and $(\bar{2}01)$ due to Ag_2MoO_4 nanophase[17–20] are present in the heat-treated sample $x=0.3$ [Fig. 1, curve e]. In Fig. 1 (curve f), the heat-treated sample $x=0.4$ shows (220), $(\bar{2}01)$, (511), and (440) peaks due to Ag_2MoO_4 cubic system of $Fd\bar{3}m$ space-group structure,[17,18] (020), (200), $(\bar{1}03)$, and

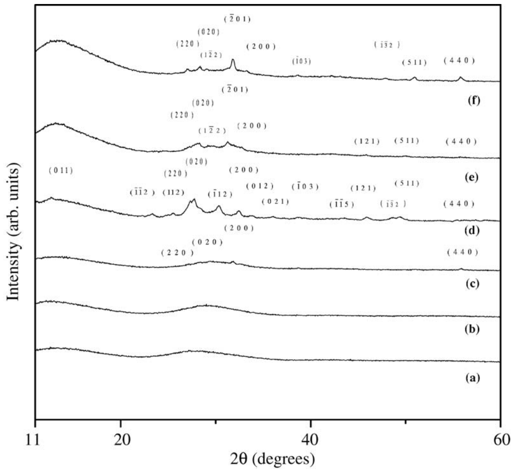

FIG. 1. XRD patterns of the as-prepared and the heat-treated samples. Curves a, b, and c correspond to the as-prepared samples $x=0.2$, 0.3, and 0.4, respectively, and curves d, e, and f correspond to heat-treated samples $x=0.2$, 0.3, and 0.4, respectively.

($\bar{1}\bar{3}2$) peaks due to $Ag_2Mo_2O_7$.[19,20] It may be noted that the $Ag_6Mo_{10}O_{33}$ nanophase present in the composition $x=0.2$ is absent in the compositions $x=0.3$ and 0.4 [Fig. 1 (curves e and f)]. In fact, all the glasses contain partial crystallinity, which could not be detected in the x-ray-diffraction (XRD) study, but are determined by the high-resolution transmission electron microscopy (HR-TEM) and field-emission scanning electron microscopy (FE-SEM) studies.

Crystallite size and the lattice strain of the nanocrystal have been evaluated using Hall's equation,[21]

$$\beta_{hkl} \cos \theta/\lambda = 2\eta \sin \theta/\lambda + K/D, \qquad (1)$$

where β_{hkl} is the full width at half maximum of a given (hkl) diffraction peak, λ is the wavelength of the x ray, D is the crystallite size, η is the measure of the heterogeneous lattice strain, θ is the Bragg angle, and K is equal to 0.9. The values of β_{hkl} were determined from the Gaussian fit to the major diffraction peaks for the heat-treated samples. The values of η were obtained from the slopes of the $\beta_{hkl} \cos \theta/\lambda$ versus $\sin \theta/\lambda$ plots [Eq. (1)]. It is clear from the analysis that the heat-treated sample $x=0.4$ has smaller lattice strain than those for the samples $x=0.2$ and 0.3. Due to the larger lattice strain in the heat-treated samples $x=0.2$ and 0.3, the probability of distribution of Ag_2MoO_4 nanoparticles is greater than that for the sample $x=0.4$. Smaller lattice strain makes the tendency of assembling the Ag_2MoO_4 nanoparticles to form clusters for heat-treated sample $x=0.4$. Such a large lattice strain in the heat-treated samples $x=0.2$ and 0.3 must be caused by the stress at the interface between the nanocrystals and the glass matrix.

The crystalline volume fraction in the heat-treated samples was determined from the following relation:[22]

$$X_{XRD}^{hkl} = I_{hkl}/(I_a + k_{hkl} I_{hkl}). \qquad (2)$$

Here, I_{hkl} represents the area under the (hkl) crystalline diffraction peak, and I_a was chosen as the area under the first diffraction maximum of the XRD under consideration. The calibration constant k_{hkl} was chosen as $k_{hkl}=I_{hkl}/I_a$. The crystalline volume fractions (X_{XRD}^{hkl}) of the heat-treated sample $x=0.2$ are found to be 0.50, 0.24, 0.15, and 0.14 corresponding to $Ag_2Mo_2O_7$ nanocrystals with (020), ($\bar{1}$12), and (200) and Ag_2MoO_4 cubic system with (511), respectively. The values of X_{XRD}^{020} and $X_{XRD}^{\bar{2}01}$, calculated for the two strongest peaks (020) and ($\bar{2}$01) for heat-treated sample $x=0.3$ [Fig. 1 (curve e)] due to $Ag_2Mo_2O_7$ nanocrystals and Ag_2MoO_4 nanophase, are 0.50 and 0.44, respectively. The values of X_{XRD}^{hkl} corresponding to Ag_2MoO_4 cubic system with (220), ($\bar{2}$01), (511), and (440) and $Ag_2Mo_2O_7$ nanocrystals with (020) are evaluated as 0.21, 0.50, 0.27, 0.35, and 0.27, respectively, for the heat-treated sample $x=0.4$. It is noteworthy that the maximum crystallinity grows inside the glass matrix corresponding to the peaks at the lower angle for the samples $x=0.2$ and 0.3, as shown in Fig. 1. However, the crystallinity grows uniformly for the heat-treated sample $x=0.4$ due to the smaller values of crystalline lattice strain, as mentioned above.

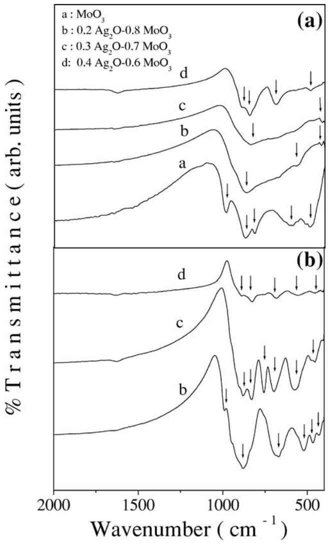

FIG. 2. (a) FT-IR spectra of the as-prepared samples and crystalline MoO_3. Curve a for MoO_3, curve b for $x=0.2$, curve c for $x=0.3$, and curve d for $x=0.4$. (b) FT-IR spectra for heat-treated samples. Curve b for $x=0.2$, curve c for $x=0.3$, and curve d for $x=0.4$.

FT-IR spectra have been used to elucidate the structural group of the glass-forming elements and are shown for all glass compositions and for their heat-treated counterparts in Figs. 2(a) and 2(b), respectively. In Fig. 2(a), FT-IR spectra of the crystalline MoO_3 are included for comparison. The most prominent absorption band at 871 cm^{-1}, observed in Fig. 2(a) for crystalline MoO_3 due to the symmetric stretching[18] of Mo-O octahedral unit, is shifted toward lower wave number when Ag_2O is introduced. The shift of the above peak indicates that the bond strength of Mo-O in glass compositions becomes weaker with the increase of Ag_2O content due to the presence of partial covalency[12] in $Ag^+ \ldots$O-Mo. The bands at 985 and 783 cm^{-1} assigned to be ν_1 and ν_3 stretching vibrations and 490 cm^{-1} assigned to be $Mo_2O_7^{2-}$ ions[23] of crystalline MoO_3 are shifted toward lower wave numbers only for composition $x=0.4$ [Fig. 2(a) (curve

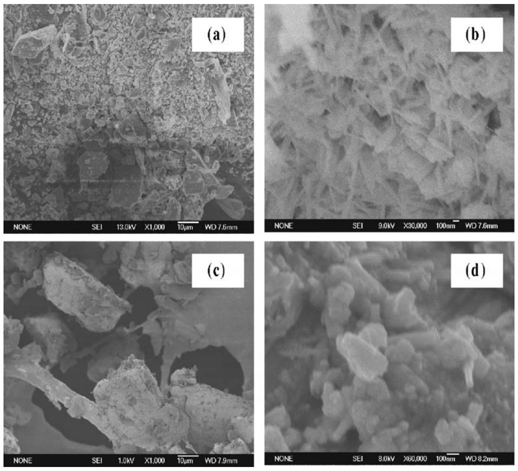

FIG. 3. (a), (b), and (c) denote, respectively, the FE-SEM images of the as-prepared samples for $x=0.2$, 0.3, and 0.4 and (d) indicates the FE-SEM image of heat-treated sample $x=0.3$.

d)] and are absent in the spectra for $x=0.2$ and 0.3. The shifting of the peaks for the composition $x=0.4$ is due to the formation of Ag_2MoO_4 nanoparticles and $Ag_2Mo_2O_7$ nanorods embedded in the glass matrix as confirmed from the x-ray-diffraction patterns. The band at 600 cm^{-1} of MoO_3 shifted toward lower wave numbers for the composition $x=0.2$ [Fig. 2(a) (curve b)] and disappears for the composition $x=0.3$ and 0.4. Similarly, the band at 416 cm^{-1} of MoO_3 due to the presence of MoO_4^{2-} anions[24] is shifted toward lower wave numbers, as shown in Fig. 2(a) (curves b and c). In Fig. 2(b), the band at 877 cm^{-1} assigned to ν_1 modes of monomeric tetrahedral orthomolybdate ion MoO_4^{2-} (Ref. 15) is not shifted for all heat-treated compositions due to the invariance of Mo-O bond length. In fact, the most prominent band at ~ 868 cm^{-1} of the original samples [Fig. 2(a)] is shifted to 877 cm^{-1} for the heat-treated samples [Fig. 2(b)] due to the enhancement of bond length. A number of new bands are formed in the heat-treated samples in the lower wave-number region [Fig. 2(b)] due to the formation of new nanophases embedded in the glass matrix. New features are observed in the spectra for the band at ~ 700 cm^{-1} [Fig. 2(b)] which lies in the vicinity of the Mo-O-Mo vibrations present in the FT-IR spectra of $K_2Mo_2O_7$ crystals.[15] This result suggests that, as the MoO_3 content of the glass nanocomposites is increased, the monomeric MoO_4^{2-} ions are successively replaced by more complex structural units containing interlinked octahedral MoO_6 and MoO_4 species.[15] Furthermore, the positions at ~ 550 and 460 cm^{-1} [Fig. 2(b)] of heat-treated samples are in agreement with the spectrum of crystalline[15] $Na_2Mo_2O_7$, suggesting that the molybdenum species in the glass nanocomposites have a similar coordination environment.

Figures 3(a)–3(c) show the FE-SEM images for the glass compositions $x=0.2$, 0.3, and 0.4, respectively, and Fig. 3(d) shows that of a typical heat-treated sample $x=0.3$. FE-SEM images exhibit the surface morphology as well as the distribution of nanoparticles and nanorods having different sizes and shapes. Ag_2MoO_4 nanoparticles with a diameter of ~ 100 nm are observed in Fig. 3(a). Figure 3(b) shows the $Ag_2Mo_2O_7$ nanorodlike structure of ~ 300 nm in length and ~ 15 nm in diameter, and microclusters of ~ 6 μm in length and ~ 2 μm in diameter size of Ag_2MoO_4 are found in Fig. 3(c). The growth of size and change in shape of the heat-treated sample is observed in Fig. 3(d) in which the length of the nanorodlike structure remains the same but its size increases radially, varying from 50 to 100 nm and some of them becoming deformed in shape.

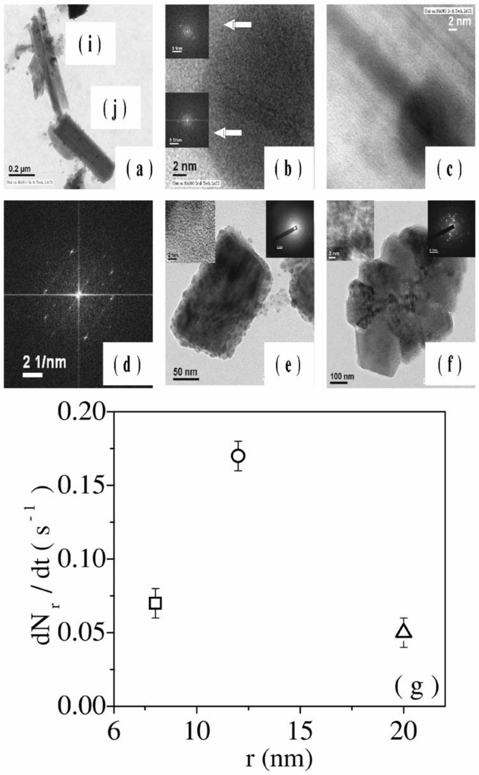

FIG. 4. (a) TEM image of heat-treated sample for $x=0.2$. Sections i and j indicate distribution of two types of nanocrystals. (b) High-resolution TEM picture of section i of (a) and their FFT (shown in the inset), indicating interplandr spacing of Ag_2MoO_4 and $Ag_2Mo_2O_7$ nanocrystals. (c) High-resolution TEM picture of section j of (a), demonstrating the $Ag_6Mo_{10}O_{33}$ nanowire. (d) FFT of (c) indicating perfect single crystal. (e) TEM image of heat-treated sample for $x=0.3$ and high-resolution TEM profile (shown in the left inset) and SAED pattern (shown in the right inset). (f) TEM image of heat-treated sample for $x=0.4$ high-resolution TEM profile (shown in the left inset) and SAED pattern (shown in the right inset). (g) The variation of growth rate of Ag_2MoO_4 nanoparticles with radius of the silver molybdate nanoparticle: □ for $x=0.2$, ○ for $x=0.3$, △ for $x=0.4$.

HR-TEM, selected area electron diffraction (SAED), and corresponding fast Fourier transform (FFT) pattern are shown in Figs. 4(a)–4(f). Figures 4(a)–4(d) describe the different sections of heat-treated sample $x=0.2$. The TEM image of the heat-treated composition $x=0.2$ exhibits two types of distribution. In Fig. 4(a), we observe the Ag_2MoO_4 nanoparticles with a diameter of ~ 100 nm and rodlike Ag_2MoO_4 (section i) and rodlike $Ag_2Mo_2O_7$ structures (section j) having a length of 300 nm and a breadth of 100 nm. High-resolution picture and corresponding FFT of Fig. 4(a) (section i) are demonstrated in Fig. 4(b), whose lattice spacings are in good agreement with those obtained from the ASTM and JCPDS data.[19] Surprisingly, crystallization is prevented around the nanophase, as shown in Fig. 4(b), due to the difference in lattice mismatch between them. The high-resolution view of Fig. 4(a) (section j) and corresponding FFT are shown in Figs. 4(c) and 4(d), respectively, which is due to the growth of single crystalline $Ag_6Mo_{10}O_{33}$ nanowires,[20] consistent with lower angle peak position in XRD [Fig. 1 (curve d)]. Figures 4(e) and 4(f) describe the TEM images of the heat-treated samples $x=0.3$ and 0.4, respectively. Sharp ring patterns, indicative of very fine nanodots without any texture,[25] and fine spot patterns, indicative of polycrystalline structure with larger grain size,[25] are observed in the inset of Figs. 4(e) and 4(f), respectively. In Figs. 4(e) and 4(f), it is noted that Ag_2MoO_4 nanoparticles with sizes of 5–7 nm are distributed on the surface of Ag_2MoO_4 and $Ag_2Mo_2O_7$ nanoclusters of definite shape. It is noteworthy that applying similar heat treatment to all the host glass nanocomposites, the formation of rodlike and nanowires are obtained due to the different stoichiometries of Ag_2O and MoO_3.

Thus, a series of TEM images [Figs. 4(a)–4(f)] recorded for the three different heat-treated samples shows the formation process of Ag_2MoO_4 nanoparticles, $Ag_2Mo_2O_7$ nanorods, and $Ag_6Mo_{10}O_{33}$ nanowires in the host glass matrices. During heat treatment, nucleation starts above T_g and the structure of nanorods is found to collapse and the widths of the nanorods increase significantly, while their lengths remain the same [Figs. 4(e) and 4(f)]. We consider that the surface melting and sublimation of nanorods induce shape transformation, as pointed out earlier.[26] The initial rapid growth of the nanoparticles and nanorods is due to the contribution of the diffusion of atoms in the glass matrices, which follows the hit-and-stick model,[26] given by

$$\frac{dN_r}{dt} = (2\pi r \sin\theta)N_0 k_d - 4\pi r^2 \alpha \rho_s k_s, \tag{3}$$

where N_r is the net growth of the number of atoms in the spherical particle of radius r and θ is the angle that specifies the degree of contact of the particles with the substrate. k_d and k_s are the diffusion rate constant and sublimation rate constant, respectively, N_0 is the steady-state concentration of the atoms on the surface, α is a factor representing the fraction of exposed surface area, and ρ_s is the surface density of the particles. Initially, the diffusion term is dominant, resulting in a rapid growth of the particles. As the particles grow in size, the sublimation term increases because of the r^2 term. When the two terms are equal, a steady state is reached achieving a maximum radius at this temperature. The values of the growth rate of nanoparticles determined from the equal area of the TEM profile for the original and heat-treated samples, respectively, are plotted with composition in Fig. 4(g). The growth rate is found to be highest for the sample $x=0.3$ and lowest for $x=0.4$. The rate of formation of Ag_2MoO_4 nanoparticles is found to be larger for $x=0.2$ and 0.3 due to their greater lattice strain, and its value becomes lower for $x=0.4$ because of its smaller lattice strain, and the Ag_2MoO_4 nanoparticles eventually take part in the formation of different silver molybdate nanoclusters and nanorods, as mentioned in the previous section.

We have observed the formation of single-crystalline $Ag_6Mo_{10}O_{33}$ nanowires in heat-treated sample $x=0.2$. The heat-treated samples $x=0.3$ and 0.4 are good templates for the formation of Ag_2MoO_4 nanoparticles and $Ag_2Mo_2O_7$ nanorodlike structures of definite geometric shape. The crystalline lattice strain of the heat-treated samples demonstrates the interface-interaction between the nanocrystals and the glass matrix. The length of the nanophase materials does not change effectively but the change in their shape is noteworthy with the increase of Ag_2O content. The hit-and-stick model can explain the initial rapid growth of the nanoparticles and nanorods in the glass matrices. The discovery of another family of molybdate nanoparticles, nanowire, and nanorodlike structures might lead to other applications of these materials and increase the scientific interests in these materials.

The authors acknowledge the support given by the Department of Science and Technology, Government of India under its Nano Science and Technology Initiative. The partial financial support by the DAE (Sanction No. 2002/37/32/BRNS), Government of India is also thankfully acknowledged.

---

*Corresponding author. Electronic address: sspag@iacs.res.in

[1] Z. Siwy *et al.*, Phys. Rev. Lett. **94**, 048102 (2005).
[2] M. Endo *et al.*, Nature (London) **433**, 476 (2005).
[3] H. Fan *et al.*, Science **304**, 567 (2004).
[4] X. W. Lou and H. C. Zeng, Chem. Mater. **14**, 4781 (2002).
[5] T. Oi *et al.*, Appl. Phys. Lett. **36**, 278 (1980).
[6] L. G. Van Uitert and S. Preziosi, J. Appl. Phys. **33**, 2908 (1962).
[7] J. G. Rushbrooke *et al.*, Nucl. Instrum. Methods Phys. Res. A **280**, 83 (1989).
[8] W. Qu *et al.*, Sens. Actuators B **64**, 76 (2000).
[9] D. Dutta and A. Ghosh, Phys. Rev. B **72**, 024201 (2005).
[10] R. Gopalakrishnan *et al.*, Mater. Res. Bull. **26**, 1371 (1991).
[11] K. Matusita, J. Ceram. Soc. Jpn. **84**, 496 (1976).
[12] T. Minami and M. Tanaka, J. Non-Cryst. Solids **38/39**, 289 (1980); T. Minami *et al.*, *ibid.* **29**, 389 (1978).
[13] S. Muto *et al.*, Solid State Ionics **35**, 307 (1989).
[14] K. Suzuki, J. Non-Cryst. Solids **192/193**, 1 (1995).
[15] N. Machida and H. Eckert, Solid State Ionics **107**, 255 (1998).
[16] M. D. Ingram *et al.*, Solid State Ionics **28-30**, 677 (1988).
[17] B. M. Gatehouse *et al.*, J. Solid State Chem. **1**, 484 (1970).
[18] A. Dalvi and K. Shahi, J. Phys. Chem. Solids **64**, 813 (2003); B. B. Das and R. Ambika, Chem. Phys. Lett. **370**, 670 (2003).
[19] ASTM Powder Diffraction File No. P-401 (unpublished); JCPDS Card No. 08-0473 (unpublished); JCPDS Card No. 75-1505 (unpublished); JCPDS Card No. 72-1689 (unpublished).
[20] X. Cui *et al.*, Chem.-Eur. J. **10**, 218 (2004).
[21] W. H. Hall, J. Inst. Met. **75**, 1127 (1950).
[22] M. Luysberg *et al.*, Philos. Mag. A **75**, 31 (1997).
[23] A. Latia *et al.*, J. Optoelectron. Adv. Mater. **5**, 185 (2003).
[24] R. A. Nyquist and R. O. Kagel, *Infrared Spectra of Inorganic Compounds*, 1st ed., (Academic, New York, 1973), p. 337.
[25] F. Yun *et al.*, Thin Solid Films **375**, 137 (2000).
[26] Z. L. Wang *et al.*, *Handbook of Nanophase and Nanostructured Materials* (Kluwer Academic, New York, 2003), Vol. 2, p. 65.